Topological analysis of SARS CoV-2 main protease

Cite as: Chaos **30**, 061102 (2020); doi: 10.1063/5.0013029
Submitted: 7 May 2020 · Accepted: 21 May 2020 ·
Published Online: 9 June 2020

Ernesto Estrada[a)]

AFFILIATIONS

Institute of Applied Mathematics (IUMA), Universidad de Zaragoza, Pedro Cerbuna 12, E-50009 Zaragoza, Spain and ARAID Foundation, Government of Aragón, 50018 Zaragoza, Spain

[a)]**Author to whom correspondence should be addressed:** estrada66@unizar.es

ABSTRACT

There is an urgent necessity of effective medication against severe acute respiratory syndrome coronavirus 2 (SARS CoV-2), which is producing the COVID-19 pandemic across the world. Its main protease (M^{pro}) represents an attractive pharmacological target due to its involvement in essential viral functions. The crystal structure of free M^{pro} shows a large structural resemblance with the main protease of SARS CoV (nowadays known as SARS CoV-1). Here, we report that average SARS CoV-2 M^{pro} is 1900% more sensitive than SARS CoV-1 M^{pro} in transmitting tiny structural changes across the whole protein through long-range interactions. The largest sensitivity of M^{pro} to structural perturbations is located exactly around the catalytic site Cys-145 and coincides with the binding site of strong inhibitors. These findings, based on a simplified representation of the protein as a residue network, may help in designing potent inhibitors of SARS CoV-2 M^{pro}.

The main protease of the new coronavirus SARS CoV-2 (severe acute respiratory syndrome coronavirus 2) represents one of the most important targets for the antiviral pharmacological actions against COVID-19. This enzyme is essential for the virus due to its proteolytic processing of polyproteins. Here, we discover that the main protease of SARS CoV-2 is topologically very similar to that of the SARS CoV-1. This is not surprising taking into account that both proteases differ only in 12 amino acids. However, we remarkably found a topological property of SARS CoV-2 that has increased more than 1900% in respect to its SARS CoV-1 analog. This property reflects the capacity of the new protease of transmitting perturbations across its domains using long-range interactions. Also remarkable is the fact that the amino acids displaying such increased sensitivity to perturbations are around the binding site of the new protease and close to its catalytic site. We also show that this sensitivity to perturbations is related to the effects of powerful protease inhibitors. In fact, the strongest inhibitors of the SARS CoV-2 main protease are those that produce the least change of this capacity of transmitting perturbations across the protein. We think that these findings may help in the design of new potent anti-SARS CoV-2 inhibitors.

I. INTRODUCTION

Since December 2019, an outbreak of pulmonary disease has been expanding from the city of Wuhan, Hubei Province, China.[1,2] This disease—produced by a new coronavirus named SARS-CoV-2[3]—has become a pandemic in about three months, affecting more than 200 countries around the world. SARS-CoV-2 belongs to the genus *Betacoronavirus*,[4,5] to which the virus that produced the respiratory epidemic of 2003 (nowadays known as SARS-CoV-1) also belongs to. The new coronavirus shares about 82% of its genome with SARS CoV-1. In spite of this similarity and of the fact that SARS-CoV-1 appeared almost 20 years ago, there are currently no approved specific drugs against SARS-CoV-2.[6–9] In consequence, most of the clinical treatment used against the disease is symptomatic in combination with some repurposed drugs, such as the antiviral remdesivir or the antimalarials chloroquine[10] and hydroxychloroquine.[11] This situation urges the scientific community to search for specific antiviral therapeutics and vaccines against SARS-CoV-2.

An attractive pharmacological target against the novel coronavirus is its viral protease, also known as the main protease (M^{pro}) of SARS CoV-2. It is a key enzyme for the virus because it is

essential for proteolytic processing of polyproteins.[12] As remarked by Zhang *et al.*,[13] "inhibiting the activity of this enzyme would block viral replication. Since no human proteases with a similar cleavage specificity are known, inhibitors are unlikely to be toxic." The three-dimensional structure of SARS CoV-2 M^{pro} has been resolved at different resolutions.[13–15] Other structures of SARS CoV-2 M^{pro} complexed with inhibitors have also been reported in recent works.[13,16,17]

There are some remarkable characteristics of SARS CoV-2 M^{pro} in relation to the protease of SARS CoV-1. They share 96% of the sequence of amino acids; i.e., they differ in the amino acids at only 12 out of 303 positions in the sequence. Zhang *et al.*[13] have reported that the superposition of the chain A of two structures corresponding to the main proteases of SARS CoV-1 and of SARS CoV-2, namely, 2BX4 and 6Y2E, respectively, shows a root mean square (r.m.s.) deviation of only 0.53 Å for all C_α positions. The first question that emerges here is whether such similarities are also reflected at the topological structural level of the proteins. By topological we mean here the discrete topology emerging from a network theoretic representation of a protein. In this representation of the protein structure, the nodes of the network represent amino acids, and the edges connecting them indicate that the corresponding residues are at a distance in which they can interact with each other. Because the Euclidean distance between the amino acids is used to construct the network, we more correctly should refer to this framework as topographical more than topological. This network theoretic representation has been previously used to answer several questions related to the protein structure and functioning.[18–22] Among the tools in use, the one of node centrality[23,24] has played a fundamental role (see, for instance, Ref. 22). These indices capture the relative importance—both structural and dynamical—of an individual amino acid in the protein.

The current study is framed in the field of analysis of complex systems related to real-world problems. These systems cover a wide range of scales that goes from the molecular to the social and ecological ones. Many efforts have been dedicated to the analysis of these systems at the largest scale, which include, for instance, crowd disasters, crime, terrorism, war, and disease spreading (see Ref. 25 and references therein). In the case of the COVID-19 pandemic, most of these efforts have been directed to the analysis of the epidemic spread.[26–30] Here, we zoom into the molecular level by constructing protein residue networks (PRNs) for SARS CoV-2 M^{pro} and some of its inhibitors. The PRN of SARS CoV-2 M^{pro} is illustrated in Fig. 1. We then analyze the similarities in the topological structure of SARS CoV-2 M^{pro} with that of SARS CoV-1 for which we also construct the corresponding PRN. We then show that both proteases are very similar in relation to a few topological characteristics, which account for a very close environment around the amino acids. That is, when the measures used account for the locality of the topological environment of a residue, the two proteases do not differ in more than 2%. However, when the measures considered account for wider environments around the nodes, the difference between the two proteins can increase up to 10%–20%. These measures quantify how a perturbation at an amino acid is transmitted through the whole structure to the rest of the residues in the protein. When this transmission is allowed not only between close pairs of amino acids but also between very distant ones, the difference between the two proteases increases up to 1900%. That is, SARS CoV-2 M^{pro} is 1900%

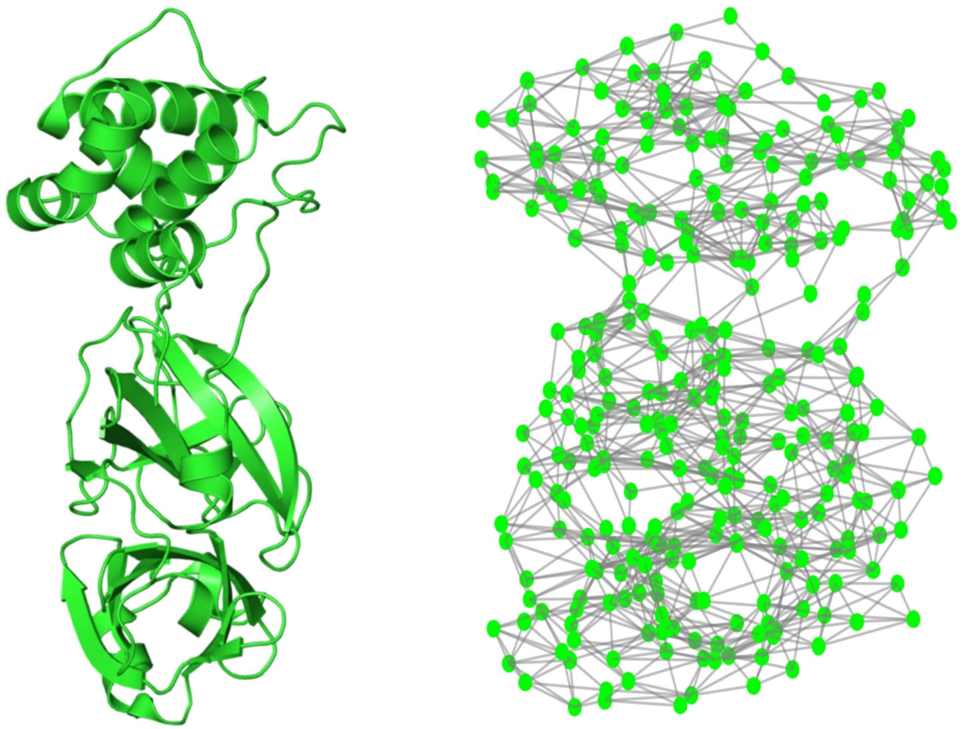

FIG. 1. Cartoon representation (left) of the M^{pro} of SARS CoV-2 (PDB = 6Y2E) and the corresponding protein residue network (right).

more sensitive to the transmission of perturbations between amino acids through the topological structure of the protein than SARS CoV-1 M^{pro}. We discovered that the residues with this largest sensitivity in SARS CoV-2 M^{pro} are the ones involved in the binding site of the three inhibitors studied here. That is, the most central amino acids according to this long-range indices are also the most affected by the interaction with the inhibitors as they are either in the binding site or very close to it. Consequently, we have discovered that the most relevant amino acids from the topological point of view are also the most relevant ones for the binding of some inhibitors to the SARS CoV-2 M^{pro} and should play an important role in the design of drugs inhibiting this protease.

II. METHODS

A. Construction of the protein residue networks

The protein residue networks (PRNs) (see Ref. 23, Chap. 14 for details) are built here by using the information reported on the Protein Data Bank[31] for the proteases of SARS CoV-1 and SARS CoV-2 as well as the complexes of the last one with three inhibitors. The nodes of the network represent the α-carbon of the amino acids. Then, we consider the cutoff radius r_C, which represents an upper limit for the separation between two residues in contact. The distance r_{ij} between two residues i and j is measured by taking the distance between C_α atoms of both residues. Then, when the inter-residue distance is equal or less than r_C, both residues are considered to be interacting and they are connected in the PRN. The adjacency matrix A of the PRN is then built with elements defined by

$$A_{ij} = \begin{cases} H\left(r_C - r_{ij}\right) & i \neq j, \\ 0 & i = j, \end{cases} \tag{1}$$

where $H(x)$ is the Heaviside function. Here, we use the typical interaction distance between two amino acids, which is equal to 7.0 Å. We have tested distances below and over this threshold obtaining in general networks, which are either too sparse or too dense, respectively.

In this work, we consider the structures of the M^{pro} of SARS CoV-1 deposited in the PDB with codes: 2H2Z,[32] 2DUC,[33] 1UJ1,[34] and 2BX4.[35] We also study the following structures of SARS CoV-2 with PDB codes: 6M03,[14] 6M2Q,[14] and 6Y2E.[13] For the complexes of M^{pro} of SARS CoV-2 with inhibitors, we study the structures with PDB codes: 6M0K,[17] 6YZE,[17] and 6Y2G.[13]

The length of the proteases is 306 amino acids. However, there are structures (see Table I) that are only resolved for amino acids 3–300, which gives a length of 298.[35] Thus, for the sake of homogeneity of the analysis, we consider here the same part of the amino acid sequence for all the structures analyzed, i.e., from residue 3 to residue 300. This does not alter the analysis as the two extremes of the protease are disordered and do not participate in important interactions.

B. Network measures

1. First category of measures

The first category of measures corresponds to those related to the most local structure around the nodes, such as those based on the degree of the nodes, i.e., the number of connections that a node has (see Ref. 23 for details). The degree accounts for the immediate effect of a node to its closest neighborhood. Among these measures, we use here the edge density, which is defined as

$$\delta = \frac{2m}{n\,(n-1)}, \tag{2}$$

where m is the number of edges and n is the number of nodes. The edge density is bounded as $0 \leq \delta \leq 1$, where the lower bound is reached for a network without any edges and the upper bound is obtained for the complete graph, which is the one in which every pair of nodes is connected to each other. Because the average degree is $\langle k \rangle = \frac{2m}{n}$, the relation with the edge density is clear.

Another measure related to the degree of the nodes is the degree heterogeneity,[36]

$$\rho = \sum_{(i,j)\in E} \left(k_i^{-1/2} - k_j^{-1/2}\right)^2, \tag{3}$$

where the summation is carried out over all pairs of connected nodes in the network. The degree heterogeneity represents a measure of how heterogeneous the degrees of the nodes are.[37] A regular network, i.e., a network with all nodes of the same degree, will have $\rho = 0$, it is followed by networks with normal-like degree distributions, then networks with more heterogeneous ones, and will end up with networks in which the probability $P(k)$ of finding a node of degree k decays like a distribution of the form $P(k) \sim k^{-1}$.

The average Watts–Strogatz clustering coefficient[38] is defined as

$$\langle C \rangle = \frac{1}{n}\sum_{i=1}^{n} \frac{2t_i}{k_i\left(k_i - 1\right)}, \tag{4}$$

where t_i is the number of triangles in which the node i takes place. It accounts for the transitivity around a node, which is bounded as $0 \leq \langle C \rangle \leq 1$, where the lower bound is attained when no nodes participate in a triangle and the upper bound is obtained when all the nodes in the network participate in the maximum possible number of triangles they can form.

We use the Newman modularity index Q[39] to account for the modular structure of PRNs. It is defined as[39]

$$Q = \sum_{k=1}^{n_C} \left[\frac{|E_k|}{m} - \frac{1}{4m^2}\left(\sum_{j=1}^{n} k_j\right)^2 \right], \tag{5}$$

TABLE I. Values of the average subgraph centrality and communicability based on simple and double factorial for the two graphs illustrated in Fig. 2 and their relative difference.

Measure	Graph (a)	Graph (b)	Δ_{rel} (%)
$\langle SC \rangle$	2.4775	2.4843	0.27
$\langle G_{pq} \rangle$	0.7773	0.7766	0.09
$\langle Z_{pp} \rangle$	4.6144	4.4109	4.41
$\langle Z_{pq} \rangle$	1.0960	1.1226	2.42

where $|E_k|$ is the number of edges between nodes in the kth community of the network, m is the total number of edges in the network, and k_j is the degree of the node j. These communities were previously detected by using the Newman eigenvector method.[40] That is, we identify the communities in a network, which are the clusters of nodes having more densities of connections among them than with those not in the cluster. Once such communities are identified, we calculated the modularity of this partition. A modularity close to zero indicates that the partition found does not differ significantly from a random clustering of the nodes. A modularity close to one indicates that this partition is significantly different to a random one.

Another measure related to the degree is the degree assortativity coefficient,[41] which is the Pearson correlation coefficient of the degree–degree correlation. $r > 0$ (degree assortativity) indicates a tendency of high degree nodes to connect to other high degree ones. $r < 0$ (degree disassortativity) indicates the tendency of high degree nodes to be connected to low degree ones.

Other measures in this class assume that "information" is transmitted in the network through the topological shortest paths. The length of the shortest path is a distance $d(i,j)$ between the corresponding pairs of nodes i and j, and it is known as the shortest path distance. The average path length

$$\langle L\rangle = \frac{1}{n(n-1)}\sum_{i<j} d(i,j) \tag{6}$$

is typically used as a measure of the "small-worldness" of the network.[38] We also consider the average betweenness centrality[42]

$$\langle BC\rangle = \frac{1}{n}\sum_{i\neq k\neq j}\frac{\rho_{ikj}}{\rho_{ij}}, \tag{7}$$

where ρ_{ikj} is the number of shortest paths between the nodes i and j that cross the node k and ρ_{ij} is the total number of shortest paths that go from i to j. It accounts for the importance of a node in passing information through it to connect other pairs of nodes via the shortest path only.

2. Second category of measures

The second category of measures is formed by those that account for the transmission of information not only via the shortest paths but by using any available route that connects the corresponding pair of nodes. These measures use the concept of a walk instead of that of a path. A walk of length k in G is a set of nodes $i_1, i_2, \ldots, i_k, i_{k+1}$ such that for all $1 \le l \le k$, $(i_l, i_{l+1}) \in E$. A *closed walk* is a walk for which $i_1 = i_{k+1}$. The number of walks of the length k between the nodes i and j in a network is given by $\left(A^k\right)_{ij}$. The first of these measures considered here is the eigenvector centrality EC,[43] which is the corresponding entry of the eigenvector associated with the largest eigenvalue of A. The relation of this index with walks is given by the following. Let $N_k(i)$ be the number of walks of the length k starting at node i and ending elsewhere. Then, if the network is not bipartite, which is the case of the current work (see Chap. 5 in Ref. 23),

$$EC_i = \lim_{k\to\infty}\frac{N_k(i)}{\sum_{j=1}^{n} N_k(j)}. \tag{8}$$

That is, the eigenvector centrality of a node is the ratio of the number of walks of infinite length that start at this node to the whole number of such walks starting elsewhere. Consequently, the average eigenvector centrality $\langle EC\rangle$ accounts for the spread of information from the nodes beyond the nearest neighbors and using any infinite-length walk in the graph.

A type of measures of the second kind are based on counting all walks of any length but giving more weight to the shorter than to the longer ones. These measures are based on the following matrix function:

$$G := \sum_{k=0}^{\infty}\frac{A^k}{k!} = \exp(A), \tag{9}$$

where $\exp(A)$ is the exponential of the matrix. Then, we consider the average of the diagonal entries of this matrix, which is known as the average subgraph centrality,[44]

$$\langle SC\rangle = \frac{1}{n}\sum_{p=1}^{n} G_{pp}, \tag{10}$$

which accounts for the participation of the corresponding node in all subgraphs of the graphs, giving more weight to the shortest than to the longer ones. Such subgraphs include, for instance, edges, triangles, wedges, squares, etc. Another measure is the average of the non-diagonal entries of $\exp(A)$, which is known as the average communicability of the network,[45]

$$\langle G_{pq}\rangle = \frac{2}{n(n-1)}\sum_{p<q} G_{pq}. \tag{11}$$

It accounts for how much a pair of nodes can communicate to each other by using all potential routes available in the network but giving more weight to the shortest than to the longer ones. Finally, in this category, we include the average communicability angle,[46]

$$\langle\theta\rangle = \frac{2}{n(n-1)}\sum_{p<q}\theta_{pq}, \tag{12}$$

where the angle between a pair of nodes is defined as

$$\theta_{pq} = \cos^{-1}\left(\frac{G_{pq}}{\sqrt{G_{pp}G_{qq}}}\right). \tag{13}$$

The average communicability angle describes how efficiently a network transmits information between its pairs of nodes by using all the available routes.

3. Third category of measures

The third category of measures is formed by all-walks indices that penalize less heavily longer walks connecting pairs of nodes in a network. That is, although $G = \exp(A)$ accounts for all walks connecting every pair of nodes, it penalizes very much those walks of relatively large length and then making more emphasis in shorter walks around a given node. In order to include longer walks in the

analysis, we study the following matrix function:[47]

$$Z := \sum_{k=0}^{\infty} \frac{A^k}{k!!} = \frac{1}{2}\left[\sqrt{2\pi}\,\mathrm{erf}\left(\frac{A}{\sqrt{2}}\right) + 2I\right]\exp\left(\frac{A^2}{2}\right), \tag{14}$$

which penalizes the walks of length k not by $k!$ (simple factorial) but by $k!!$ (double factorial). The main effect of the use of this double factorial penalization instead of the simple factorial is that the walks of longer length are less penalized than when we use the simple factorial. For instance, let us consider a pair of residues in a PRN separated by 10 edges. In the communicability function, the contribution of this interaction will be 1/3 628 800, which is practically null. However, in the Z function, this contribution is 1/3848, which is almost 10^3 stronger than in the previous case.

Then, we will consider here the average of the main diagonal,

$$\langle Z_{ii}\rangle = \frac{1}{n}\sum_{i=1}^{n} Z_{ii}, \tag{15}$$

which accounts for the participation of the node i in all subgraphs in the graph but including bigger subgraphs than in SC. In a similar way, we consider

$$\langle Z_{ij}\rangle = \frac{2}{n\,(n-1)}\sum_{p<q} Z_{ij}, \tag{16}$$

which accounts for the global capacity of the network of transmitting information between pairs of nodes and allowing longer-range transmission than in the case of the communicability. For those reasons, we propose to call these indices long-range (LR) subgraph centrality and communicability, respectively.

a. Example. In order to illustrate the sensitivity of the different topological measures used here to structural changes in protein residue networks, we construct the following toy model. One of the characteristic features of protein residue networks is the presence of chordless cycles. A chordless cycle is a cycle that contains no edge, which does not itself belongs to the cycle. These chordless cycles—also known as holes or induced cycles—represent pockets in the protein, which may be involved in the binding of ligands and/or inhibitors. In Fig. 2(a), we illustrate a simple graph having two chordless cycles of six nodes each. The graph illustrated in Fig. 2(b) differs on that in (a) in which it has two holes of five and seven nodes each.

In Table I, we give the values of the average subgraph centrality and communicability based on the matrix exponential, $\langle SC\rangle$ and $\langle G_{pq}\rangle$, respectively, for the two graphs in Fig. 2. As can be seen, the subgraph centrality of both graphs differs less than 0.5% and the communicability in less than 0.1%. This is a consequence of the fact that these indices based on the matrix exponential penalize very heavily the walks of relatively large length, which means that they hardly differentiate cycles of length 5, 6, and 7. However, the two indices based on the double factorial penalization are capable to distinguish very well between these cycles and produce relative differences of almost 5% for $\langle Z_{pp}\rangle$ and of 2.4% for $\langle Z_{pq}\rangle$. As we will see later on this work, this difference between the indices based on the simple and double factorial is essential to find important amino acid contributions to the interactions of SARS CoV-2 main protease with inhibitors.

III. RESULTS

A. Free protease

The main goal of this section is to analyze a few network theoretic measures of the M^{pro} of SARS CoV-2 and compare them with those of the protease of SARS CoV-1. The amino acid sequence of both proteases shares 96% of similarity; i.e., only 12 amino acids are different in both proteases of a total of 303. These amino acids are at positions 33, 44, 63, 84, 86, 92, 132, 178, 200, 265, 283, and 284. In order to compare the topological features of the main proteases of SARS CoV-1 and of SARS CoV-2, we go a step further here and compare several structures of the M^{pro} of SARS CoV-1 and SARS CoV-2. In Table II, we give the PDB codes of six structures of the main protease of SARS CoV-1 and four of SARS CoV-2 without inhibitors. In these structures, not only there are no inhibitors, but also there are no mutations in the structure of the wild proteases. In the case of

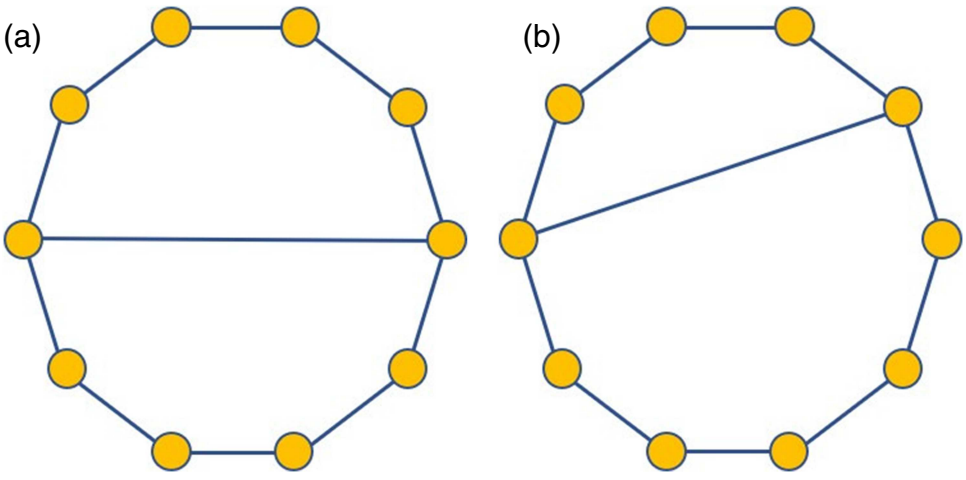

FIG. 2. Example to illustrate the sensitivity of the topological measures to structural changes in protein residue networks (see the text for explanations). (a) A graph with two chordless cycles of 6 nodes. (b) A graph with a chordless cycle of 5 nodes and another of 7 nodes.

TABLE II. Protein Data Bank codes for the structure of the main protease of SARS CoV-1 and SARS CoV-2 without inhibitors (apo forms).

SARS CoV-1			SARS CoV-2		
PDB	Res. (Å)	Length	PDB	Res. (Å)	Length
2H2Z	1.60	306	6YB7[a]	1.25	306
2DUC	1.70	306	6M2Q	1.70	305
1Q2W[b]	1.86	295	6Y2E	1.75	306
1UJ1	1.90	301	6M03	2.00	306
3VB3[c]	2.20	301			
2BX4	2.79	298			

[a]The structure 6YB7 is resolved with dimethylsulfoxide as a ligand.
[b]Residues 45–48 are missing in the crystal structure.
[c]The structure 3VB3 is resolved with two ligands; di(hydroxyethyl)ether and 1,2-ethanediol.

the structure with the PDB code 1Q2W, the residues 45–48 are missing in the PDB. In 3VB3, we have found that di(hydroxyethyl)ether (PEG) and 1,2-ethanediol (EDO) are also present in the crystal structure. In a similar way, the structure 6YB7 contains dimethylsulfoxide (DMS) in the crystal structure. For these reasons, we will not include these three structures in further analysis.

For the rest of the structures, i.e., four structures of the main protease of SARS CoV-1 and three structures of the same for SARS CoV-2, we calculate all the topological measures defined in Sec. II. We then obtained the mean and standard deviation of these measures for the two groups of structures and report them in Table III. We can observe in this table that most of the topological characteristics of the first kind of the PRNs of both proteases are very similar with relative differences not bigger than 2% for all the properties analyzed. In order to test the significance of the differences between the two groups of proteases, we use the p-values of the Mann–Whitney *U*-test.[48] This statistical measure has been proposed for the analysis of network measures, in particular, for protein networks.[49,50] According to the p-values (see the last column in Table III), none of these measures display a significant difference between the two groups of proteases.

We then continue the analysis by comparing the topological measures of the second kind. We notice that the eigenvector centrality, which has been found very useful in the previous analysis of PRN,[22] does not display any significant difference between both proteases according to the Mann–Whitney test. However, there are differences in the mean subgraph centrality of about 14% and of the average communicability between pairs of nodes of about 18%. In both cases, the indices are significantly larger for the protease of SARS CoV-2 than for that of SARS CoV-1. According to the p-values, these differences are significant at a 94% level of confidence in the Mann–Whitney *U*-test. This means that the structural changes that make the difference between the proteases of SARS CoV-1 and SARS CoV-2 increase the capacity of the individual amino acids of feeling a perturbation or thermal oscillation produced in another amino acid of the protein. As we have previously explained, these communicability factors penalize very heavily any perturbation being transmitted between two amino acids separated

TABLE III. Average values of the global topological properties of the M^{pro} of SARS CoV-1 (2H2Z, 1UJ1, 2DUC, 2BX4) and SARS CoV-2 (6M03, 6Y2E, 6M2Q). The relative difference between them, expressed as percentages of the change relative to SARS CoV-1, and the p-values of the Mann–Whitney *U*-test are also given. Boldface denotes the values with the most significant difference relative to SARS CoV-1.

Measure	SARS CoV-1	SARS CoV-2	Δ_{rel} (%)	U-stat
δ	0.0260	0.0262	−0.71	0.2286
ρ	0.0163	0.0164	−0.98	0.8571
$\langle L \rangle$	6.37	6.33	0.69	0.2286
Q	0.613	0.610	0.49	1.0000
$\langle C \rangle$	0.542	0.540	0.31	0.8571
r	0.390	0.398	−1.85	0.8571
$\langle BC \rangle$	796.29	793.76	0.32	0.6286
$\langle EC \rangle$	0.003 36	0.003 34	0.50	0.5714
$\langle SC \rangle$	172.00	196.04	**−13.97**	**0.0571**
$\langle G_{pq} \rangle$	22.42	26.46	**−18.01**	**0.0571**
$\langle \theta \rangle$	82.29	82.01	0.34	**0.0571**
$\langle Z_{pp} \rangle$	4.65×10^{17}	9.57×10^{18}	**−1960.15**	**0.0571**
$\langle Z_{pq} \rangle$	1.44×10^{17}	2.91×10^{18}	**−1921.88**	**0.0571**

by a relatively shortest path distance in the protein. Thus, they can be considered as indices that account for shorter range interactions than the third kind measures considered here. It should be noticed that although the communicability angles display very little relative variation between the two groups of proteases, these differences are significant at 94% of confidence in the Mann–Whitney test.

Both LR subgraph centrality and communicability display a dramatic increment in SARS CoV-2 relative to SARS CoV-1. In this case, the increase of these indices is more than 1900% for both, the LR communicability and the LR subgraph centrality. In short, this means that the protease of SARS CoV-2 has more than 13 times more capacity of transmitting perturbations between pairs of nodes than the protease of SARS CoV-1. This is equivalent to say that the protease of SARS CoV-2 is significantly much more topologically efficient in transmitting "information" among its amino acids than the protease of SARS CoV-1. These two topological measures display significant differences between the two groups of proteases according to the statistical p-values obtained from the Mann–Whitney *U*-test at 94% of confidence.

We now proceed to the analysis of the local variation of the subgraph and the LR subgraph centralities for the amino acids of the two M^{pro} (see Fig. 3) averaged for all the structures previously mentioned, i.e., 2H2Z, 1UJ1, 2DUC, and 2BX4 for SARS CoV-1 and 6M03, 6Y2E, and 6M2Q for SARS CoV-2. In the case of the subgraph centrality, the largest change is produced for a few amino acids, which increase their centrality in SARS CoV-2 relative to SARS CoV-1. These are the cases of residues number 25, 26, 27, 118, 17, and 24. However, there are also other amino acids that drop their centrality in SARS CoV-2, such residues number 170, 73, 169, 165, 89, and 252 among others [see Fig. 3(b)]. Therefore, the increase of the subgraph centrality of a few amino acids makes that in total, the average subgraph centrality increases in SARS CoV-2 in relation to SARS CoV-1. An important characteristic feature of the differences

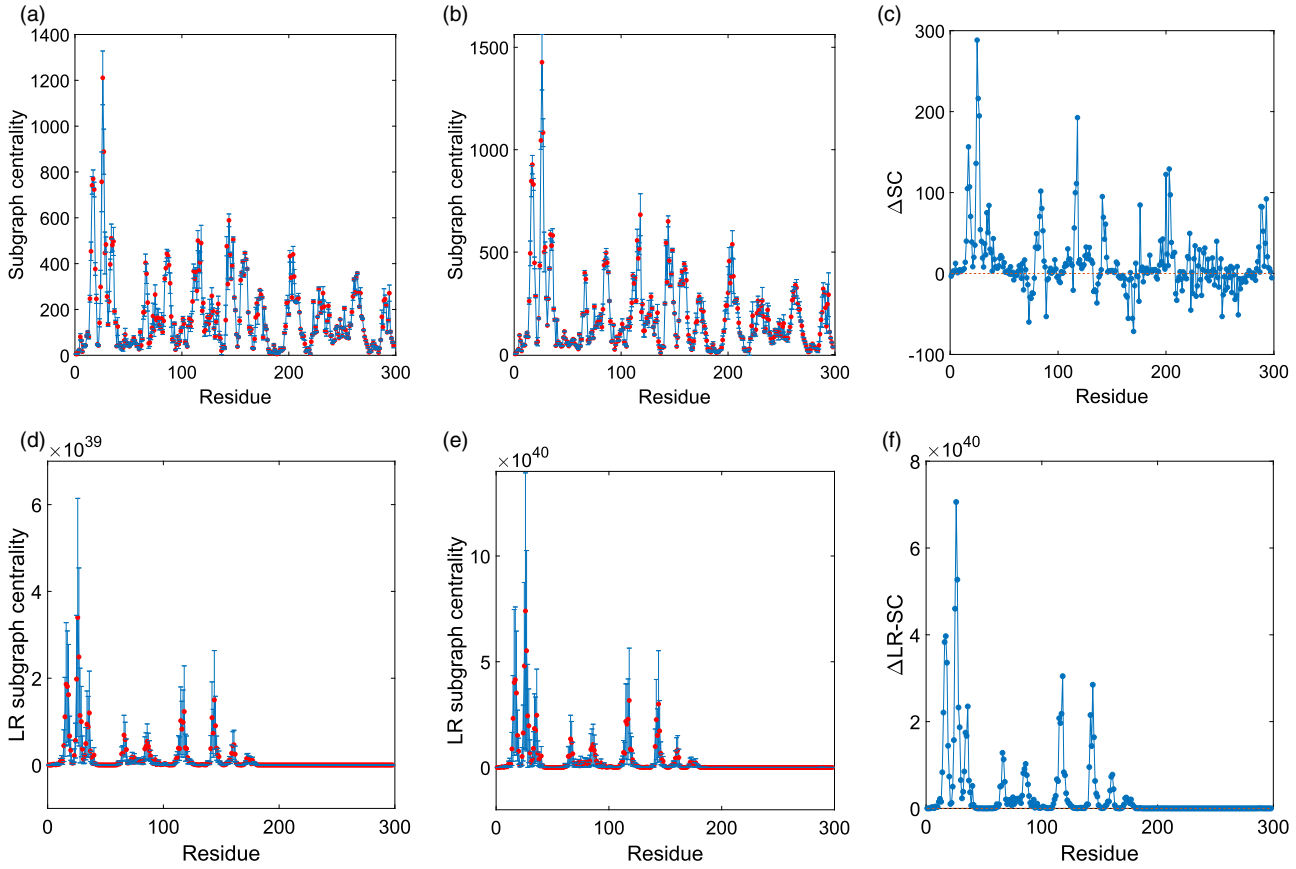

FIG. 3. Plot of subgraph centrality (a)–(c) as well as LR subgraph centrality (d)–(f) of the amino acid residues for the M^{pro} of SARS CoV-1 (a) and (d), SARS CoV-2 (b) and (e), and the difference between them (c) and (f).

in this centrality between the two proteases is that they are spread across the three domains of the proteases with a large increment in the domains I and III. This is a major difference with the LR subgraph centrality [see Figs. 3(c) and 3(d)], where the main change is a dramatic increase in the centrality of the nodes in domains I and II of the SARS CoV-2 protease relative to SARS CoV-1. The changes occurring in domain III are imperceptible in relation to those of the other two domains.[32]

In order to illustrate the distributions of the most central amino acids according to both measures in the three-dimensional structures of the proteases, we selected two structures, 2BX4 for SARS CoV-1 and 6Y2E for SARS CoV-2 as a representative of the two groups of structures. Notice that these two structures have been used by Zhang *et al.*[13] for their comparison of the 3D structures of both proteases. Both structures are illustrated in Fig. 4. It can be seen that the largest values of the LR subgraph centrality are concentrated in a relatively small region of the protein structure, while those of the subgraph centrality are more spread across the whole structure. We then inquire about this region of the M^{pro} in SARS CoV-2, which shows the largest change in the LR subgraph centrality relative to its analog of SARS CoV-1.

The first remarkable observation of the amino acids with the largest change in the LR subgraph centrality is that they are all closely located to each other in the three-dimensional space. For instance, the 22 amino acids displaying the largest change in this centrality form a connected subgraph of the PRN as illustrated in Fig. 5. This subgraph of 22 nodes has 48 connections among these amino acids, which produces an edge density of 0.21, almost 10 times bigger than the total density of the protease. The second remarkable feature of this subgraph is that it contains one of the two catalytic amino acids of the M^{pro} of SARS CoV-2, which is Cys-145. That is, the region with the largest increase in the LR subgraph centrality of the protease of SARS CoV-2 relative to SARS CoV-1 is the one enclosing the catalytic binding site of the amino acid Cys-145. It is also remarkable that this region with a large increment in the LR subgraph centrality contains some amino acids that are located in the binding site of the M^{pro} to α-ketoamide inhibitors as well as other kinds of inhibitors, as we will analyze further in this work. This is the case of the residues 144–147, and other amino acids in this binding site such as residues 162 and 163 which also display a large increment in the LR subgraph centrality. The last remarkable observation is that domain III displays a small change in

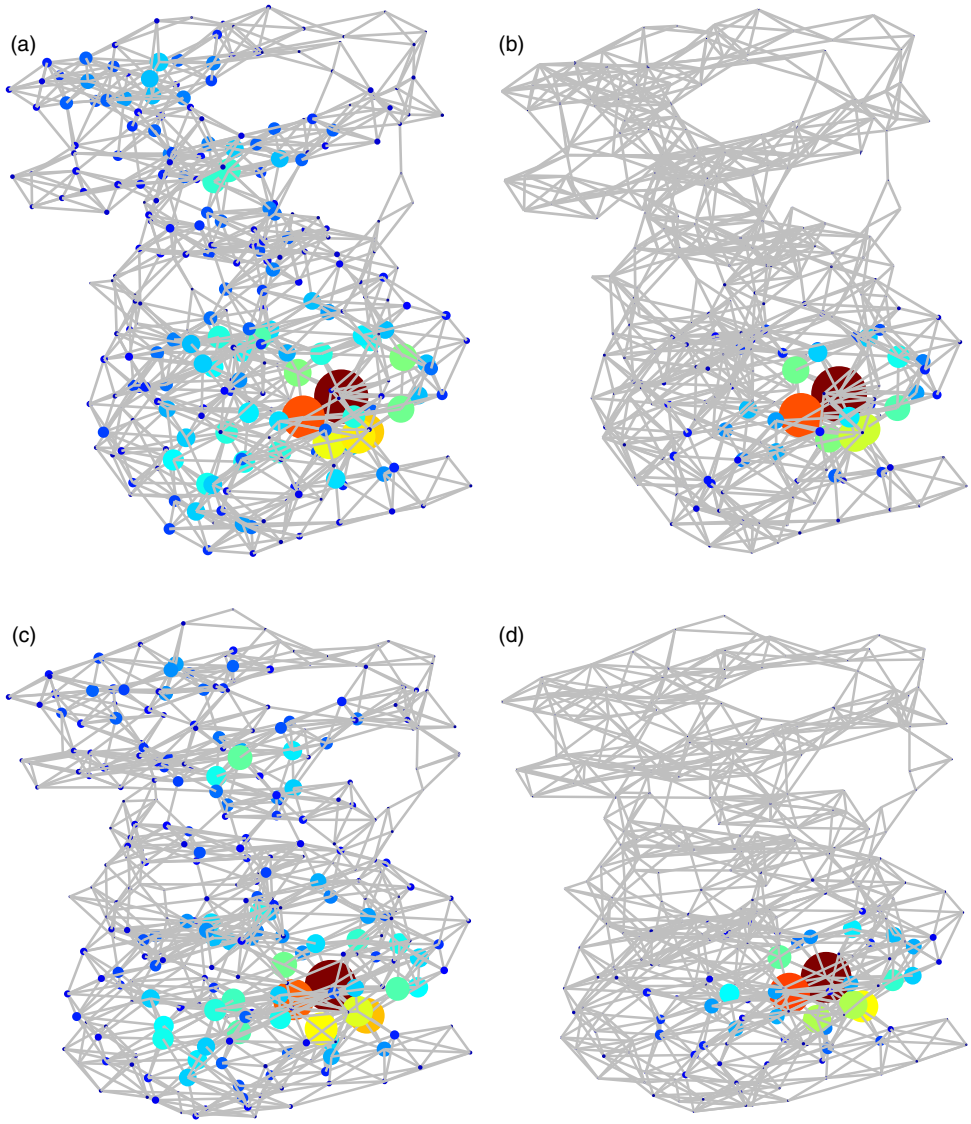

FIG. 4. Illustration of the subgraph (a) and (c) and LR subgraph (b) and (d) centralities of the amino acid residues of the chain A of SARS CoV-1 M^{pro} of (top) and of SARS CoV-2 (bottom). The size of the nodes is proportional to the corresponding centrality normalized to its largest value in the protease analyzed. The colors also correspond to the same values in the jet color code, with red for higher values and blue for smaller values.

relation to the changes of domains I and II in this topological parameter. However, as we will see in the next paragraphs, this domain (residues 198–303), which is formed by five helices and is involved in the dimerization of the M^{pro}, also increases significantly the LR communicability in relation to SARS CoV-1.

A better picture of the changes in the different regions of the M^{pro} of SARS CoV-2 relative to SARS CoV-1 can be obtained again by analyzing the differences between the communicabilities and LR-communicabilities averaged for the four structures of SARS CoV-1 and three structures of SARS CoV-2 before considered. For this, we obtain an average communicability (resp. LR communicability) matrix for the structures of SARS CoV-1 and another for the structures of SARS CoV-2. Then, we obtain the difference between these two matrices. In Fig. 6, we illustrate the difference in the matrices for both kinds of communicabilities. In the first case, it can be observed that the communicability between all pairs of residues in domain I (residues 10–99) mainly increases in SARS CoV-2 relative to SARS CoV-1, with an increase of 12.8% relative to SARS CoV-1. However, in domain II (residues 100–182), there is mainly a drop of the communicability between the residues in the domain, which decrease 2.02%, but there is an increase of 19.6% in the trade-off between domains I and II and an increase of 39.2% in the trade-off between domains I and III. The domain III shows a mixed behavior with some pairs of residues increasing and other decreasing their communicability, but the main result is an increase of 5.58% relative to SARS CoV-1. The communicability between domains II and III in the SARS CoV-2 structures increases in 23.9% relative to the same in SARS CoV-1.

We finally analyze the changes in the LR communicability between the different domains of the SARS CoV-2 protease. Here,

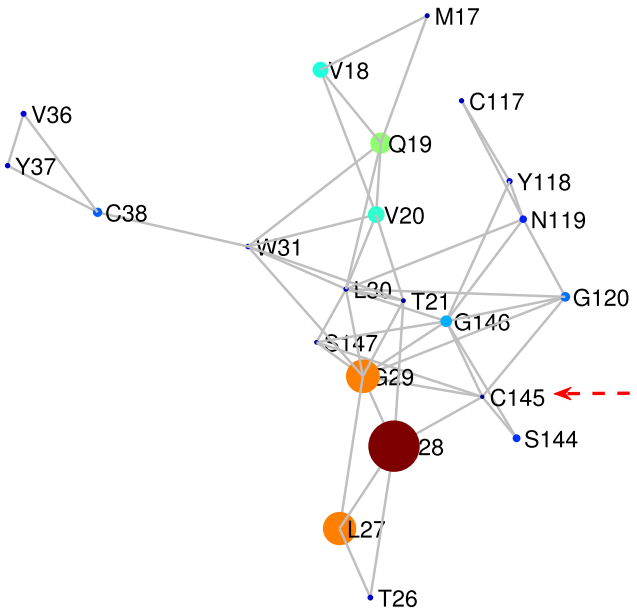

FIG. 5. Illustration of the 22 amino acids that display the largest difference in the LR subgraph centrality in a representative M^{pro} of SARS CoV-2 (6Y2E) in relation to one of SARS CoV-1 (2BX4). The radius of the nodes is proportional to the difference in the LR subgraph centrality between the two proteases. The catalytic site Cys-145 is pointed to with an arrow. The size of the nodes is proportional to the corresponding centrality normalized to its largest value in the protease analyzed. The colors also correspond to the same values in the jet color code, with red for higher values and blue for smaller values.

the changes are dramatic, and in all cases, the LR communicability in the SARS CoV-2 protease is higher than that in SARS CoV-1. For instance, the average communicability between pairs of nodes in domain I is 1997% higher in SARS CoV-2 than in SARS CoV-1. This percentage of increment is 1814% in domain II and 2651% in domain III. The inter-domain communicability also increases very significantly with an increment of 1896% (domains I and II), 2350% (domains (I–III), and 2237% (domains II and III). In closing, the structural changes between the main proteases of SARS CoV-1 and SARS CoV-2 produced a dramatic impact in the LR communicability between residues in the protease of SARS CoV-2 with a huge improvement in the long-range communication between residues practically in all domains of the protease.

TABLE IV. Relative differences in percentage of global topological properties of the M^{pro} of SARS CoV-2 complexed to an inhibitor in relation to the free one. The properties for the wild (apo form) protease correspond to the average of the 3 structures considered here (see Table III).

Measure	Wild	6M0K	6LZE	6Y2G
δ	0.0262	0.0262	0.0262	0.0255
ρ	0.0164	0.0167	0.0164	0.0178
$\langle L \rangle$	6.33	6.386	6.383	6.35
$\langle C \rangle$	0.54	0.54	0.54	0.54
r	0.398	0.394	0.375	0.37
$\langle BC \rangle$	793.76	799.86	799.39	795.92
$\langle EC \rangle$	0.003 34	0.003 35	0.003 36	0.0033
$\langle SC \rangle$	196.04	187.85	180.42	156.09
$\langle G_{pq} \rangle$	26.46	25.07	23.40	20.09
$\langle \theta \rangle$	82.01	82.12	82.24	82.45
$\langle Z_{ii} \rangle$	9.57×10^{18}	1.99×10^{18}	4.79×10^{17}	1.28×10^{17}
$\langle Z_{ij} \rangle$	2.91×10^{18}	5.93×10^{17}	1.54×10^{17}	4.06×10^{16}
IC_{50} (μM)		0.04 ± 0.002	0.053 ± 0.005	0.67 ± 0.18

B. SARS CoV-2 protease bounded to inhibitors

We turn now our attention to the analysis of the M^{pro} of SARS CoV-2 complexed with some inhibitors. The selection of these inhibitors has been based on (i) the existence of the crystallographic structure of the complex inhibitor-M^{pro}, (ii) the existence of reports about the inhibitory concentration IC_{50} of the inhibitor, and (iii) the fact that the inhibitors display a great potency against the main protease of SARS CoV-2. Then, we have selected three complexes that correspond to PDB codes 6M0K, 6LZE, and 6Y2G. The first two compounds were recently reported by Dai *et al.*[17] and the third is an α-ketoamide inhibitor reported by Zhang *et al.*[13] The first

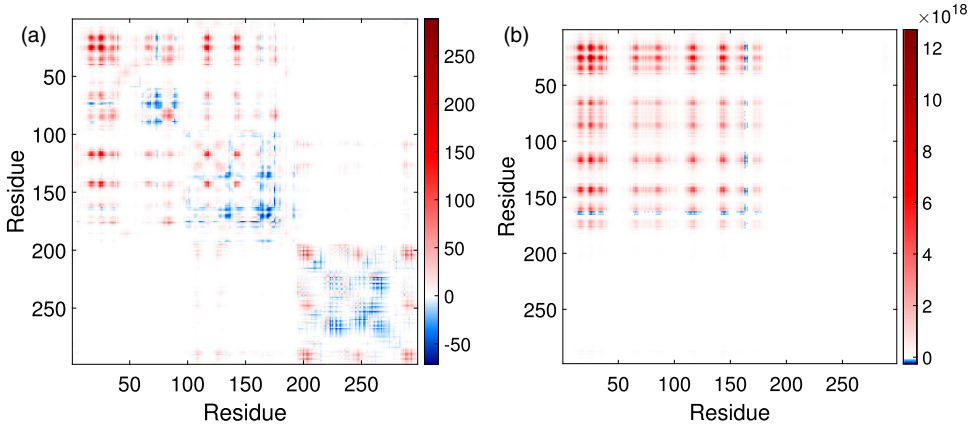

FIG. 6. Difference between communicabilities (a) and the LR communicability (b) between pairs of amino acids in the averaged structures of M^{pro} of SARS CoV-2 in relation to that of SARS CoV-1.

two inhibitors display $IC_{50} < 0.1\mu M$ and the third shows $IC_{50} \approx 0.67 \pm 0.18$.

In Table IV, we resume the results of the calculation of average topological properties of the M^{pro} structure bounded to these inhibitors. In these calculations, we consider only the residues 3–300 of the protease as explained in Sec. II to make these results comparable with the ones obtained in Sec. III A. It can be seen that here again, the topological measures of the first class display little variation for the three complexed proteases relative to the free one.

We then move to the analysis of the measures of the second and third type. As can be seen in Table IV, there are significant changes, of more than 20%, in the subgraph centrality and the communicability of the complexed proteases in relation to the average of the wild proteases previously analyzed. However, here again, the most dramatic change in these topological properties occurs in the values of the LR subgraph centrality and communicability, with relative changes of more than 98%. We should notice that the smallest change in these parameters occurs for the structure 6M0K, which corresponds to the strongest inhibitor, followed by 6LZE, which is the intermediate one, and finally 6Y2G, which is the weakest of the three. That is, the strongest inhibitor produces the smallest changes in the (LR) subgraph centrality and (LR) communicability in relation to the wild protease. In contrast, the weakest inhibitor changes most of these communicability parameters relative to the unbounded protease. These results appear to indicate that the potency of these inhibitors could be related to the fact of not affecting very much the strong inter-residue communicability of amino acids in the M^{pro} of SARS CoV-2.

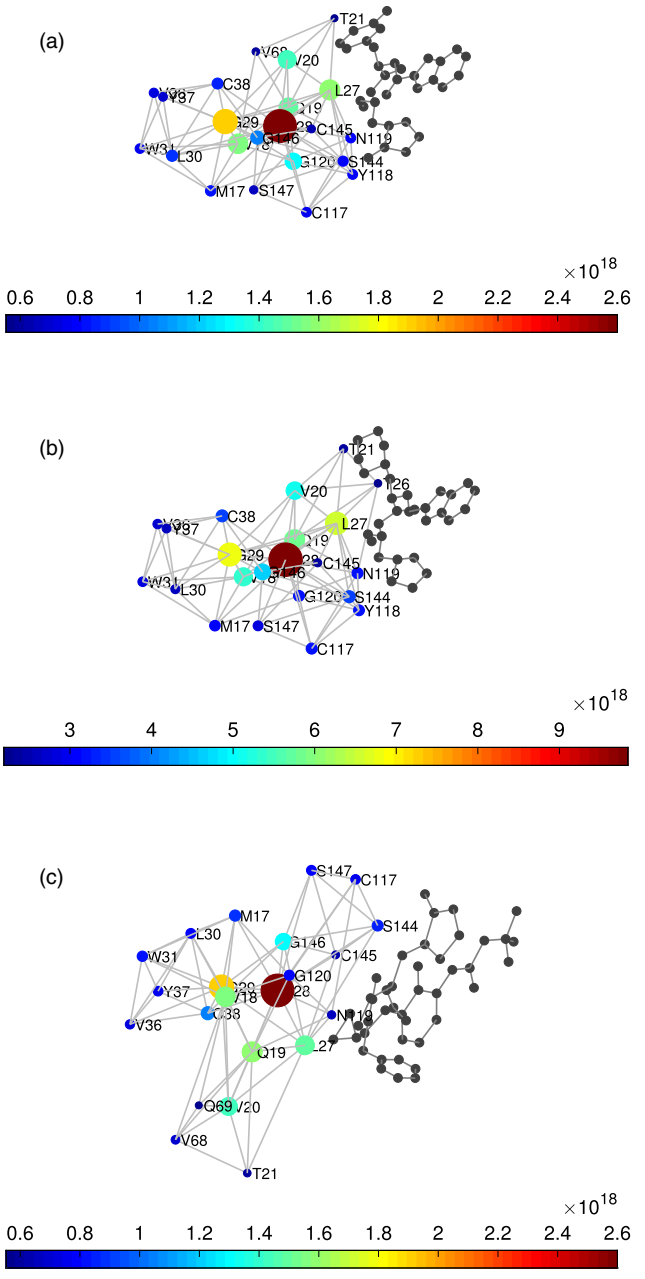

FIG. 7. Illustration of the 22 amino acids with the largest values of the LR subgraph centrality in 6M0K (a), 6LZE (b), and 6Y2G (c). The residues are connected if they are at no more than 7.0 Å. The color bar and the radius of the nodes indicate the values of Z_{ii}.

TABLE V. List of amino acids with the largest values of LR subgraph centrality in the average free protease (average of 6M03, 6Y2E, 6M2Q) and with the same parameter for the protease bounded to inhibitors (6M0K, 6LZE, and 6Y2G). The amino acids in the bounded protease that are not in the top rank of the free one are marked in bold.

Rank	Average	6M0K	6LZE	6Y2G
1	N28	N28	N28	N28
2	G29	G29	G29	G29
3	L27	L27	L27	Q19
4	V18	V18	Q19	V18
5	Q19	Q19	V18	L27
6	V20	V20	V20	V20
7	G146	G120	G146	G146
8	G120	G146	S144	C38
9	L30	L30	C38	M17
10	C38	C38	N119	S144
11	M17	M17	C117	W31
12	N119	S144	G120	G120
13	S144	N119	Y118	S147
14	Y118	Y118	M17	L30
15	C117	C117	S147	Y37
16	W31	W31	W31	C117
17	V36	V36	V36	V36
18	Y37	Y37	L30	**V68**
19	S147	S147	Y37	N119
20	T26	C145	T21	C145
21	C145	**V68**	C145	T21
22	T21	T21	T26	**Q69**

With the goal of disentangling the information contained in the changes produced at the LR subgraph centrality of the bounded protease, we study it in more detail here. For this, we consider the amino acids displaying the largest values of this topological parameter for the three structures. In Fig. 7, we illustrate the region formed by the top 22 amino acids according to their values of the Z_{ij} index, i.e., LR subgraph centrality. The first interesting observation is that for the three structures considered, these amino acids form a connected subgraph in the main protease. That is, these amino acids displaying the highest LR subgraph centrality are not randomly distributed around the domains of the protease, but they are located in a specific location of the space. It is also remarkable that this subgraph is connected, which means that there is no single amino acid separated at more than 7 Å from the rest of residues forming the subgraph. Another remarkable characteristic of these subgraphs of the most central residues according to LR subgraph centrality is that they are exactly around the binding site of the main protease. As can be seen in Fig. 7, these subgraphs of residues are very close to the inhibitors and form a cluster of amino acids around the catalytic site, which is C145.

In Table V, we resume the results of the top ranked amino acids according to the LR subgraph centrality for the free SARS CoV-2 M^{pro} taken as the average of the three apo structures previously considered and the three complexes with inhibitors studied here. As can be seen, the top 22 amino acids in the average free SARS CoV-2 M^{pro} contain more than 90% of the residues, which appear involved in the interactions with the three inhibitors studied here. In the case of 6LZE, they coincide in 100%, and in 6M0K, the coincidence is of 95%.

IV. DISCUSSION AND CONCLUSIONS

We present an analysis of some of the most relevant topological properties of the main protease of the SARS CoV-2. Our approach is based on the representation of the three-dimensional structure of the protein as a residue network in which C_α of every amino acid is represented by a node of the network and two nodes are connected if the corresponding C_α is at no more than 7.0 Å. We find here that the difference between most of the topological properties of the PRNs representing both proteases differs less than 5%. If we exclude from the analysis the LR measures, then 70% of the topological measures shows only a small variation between the two proteases taking as the average of the properties of several structures representing each of the two proteases. In this situation, it is certainly remarkable that there are topological measures that change in more than 1900% from one protease to the other. These are the cases of the LR subgraph centrality of the amino acids and of the LR communicability between pairs of them. The increase of these parameters in more than 1900% for SARS CoV-2 M^{pro} relative to SARS CoV-1 M^{pro} means that the structural changes that differentiate both proteases have created a huge increment in the efficiency of SARS CoV-2 M^{pro} in transmitting perturbations of any kind between the amino acids of the protein using all the available routes of connection and allowing for long-distance transmission. To make clearer what this sensitivity means, we are going to use a simple example. Let us consider a tiny perturbation on the structure of the proteases that prevent the interaction between the amino acids P9 and G11, which have been selected at random. In SARS CoV-1 M^{pro} (taking 2BX4 as an example), these amino acids are at 5.69 Å and in SARS CoV-2 M^{pro} (taking 6Y2E as an example), they are 6.48 Å apart. Thus, in both cases, they are connected in the corresponding PRN. Let us consider that the perturbation removes this edge from the PRN of both proteases. The relative decrement of the average path length in SARS CoV-2 M^{pro} relative to SARS CoV-1 M^{pro} is almost imperceptible, i.e., 5.7%. In the case of the subgraph centrality, it is of the same order, i.e., 3.4%. This means that according to these parameters, SARS CoV-2 M^{pro} is as sensitive as SARS CoV-1 M^{pro} to perceive a structural change in its structure produced by a given perturbation. However, when we consider the LR subgraph centrality, this relative change is 316.8%. That is, according to this topological parameter that takes into account long-range interactions, SARS CoV-2 M^{pro} is more than three times more sensitive to a tiny structural change than SARS CoV-1 M^{pro}. This remarkable finding indicates that the changes produced in SARS CoV-1 M^{pro} make the resulting SARS CoV-2 M^{pro} much more efficient in transmitting "information" through the protein skeleton using short and long-range routes.

The second remarkable finding of the current work is that the largest changes in the LR subgraph centrality occurring in SARS CoV-2 M^{pro} relative to SARS CoV-1 M^{pro} do not spread equally across the whole structure of the protease. Instead, they are concentrated around a geometrical region, which includes most of the amino acids involved in the binding site of the protease to inhibitors or close to it. One of the amino acids that has increased more dramatically its sensitivity to long-range transmission of information in SARS CoV-2 M^{pro} is Cys-145, which is one of the two catalytic sites of the protease, and the one involved in interactions with the inhibitors, such as the ones analyzed here. We have analyzed here three different inhibitors of SARS CoV-2 M^{pro} displaying very potent inhibitory capacity over the protease. In the three cases, we have observed a significant variation in the LR subgraph centrality of the amino acids, which were previously observed to have increased their LR sensitivity in the free protease. Therefore, these amino acids correspond to those involved in the binding of these three inhibitors, showing that their increased topological role in the SARS CoV-2 M^{pro} also may play an important functional role in it.

The analysis of PRN is easier than the study of the whole protein structure. In this sense, the PRN represents a simplified model of the three-dimensional structure of the protein. Typically, such simplification in the complexity of the representation of systems conveys a loss in the structural information, which is represented by the global system. In this case, however, we have shown that the use of a network representation of the proteins reveals some hidden patterns in their structure that were escaping to the analysis by using the global structure. To detect such important structural factors, it is necessary to account for long-range interactions among the amino acids of the proteases, which are the ones revealing their most important characteristics in terms of their sensitivity to tiny structural changes produced by local or global perturbations to the system. Such LR interactions revealed here the main differences between the proteases of SARS CoV-1 and SARS CoV-2, as well as the most important amino acids for the interaction with inhibitors, which may produce therapeutic candidates against COVID-19.

SUPPLEMENTARY MATERIAL

The x, y, and z coordinates of the C_α of all amino acids in the proteins studied in this work are provided in the supplementary material. We also provide the adjacency lists of the protein residue networks constructed by using a threshold radius of 7 Å. In all cases, the lists contain information for residues numbered from 3 to 300 as explained in the paper.

DATA AVAILABILITY

We provide supplementary data containing the Cartesian coordinates of the α-carbons of the residues in the proteins analyzed here as well as the adjacency lists for all these protein residue networks. Any other data can be requested by email to the author.

REFERENCES

[1] P. Zhou, X. L. Yang, X. G. Wang, B. Hu, L. Zhang, W. Zhang, H. R. Si, Y. Zhu, B. Li, C. L. Huang, and H. D. Chen, "A pneumonia outbreak associated with a new coronavirus of probable bat origin," Nature **579**, 270–273 (2020).

[2] F. Wu, S. Zhao, B. Yu, Y. M. Chen, W. Wang, Z. G. Song, Y. Hu, Z. W. Tao, J. H. Tian, Y. Y. Pei, and M. L. Yuan, "A new coronavirus associated with human respiratory disease in China," Nature **579**, 265–269 (2020).

[3] A. Gorbalenya, S. Baker, and R. Baric—Coronaviridae Study Group of the International Committee on Taxonomy of Viruses, "The species *Severe acute respiratory syndrome-related coronavirus*: Classifying 2019-nCoV and naming it SARS-CoV-2," Nat. Microbiol. **5**, 536 (2020).

[4] *Virus Taxonomy. Ninth Report of the International Committee on Taxonomy of Viruses*, edited by A. M. Q. King, M. J. Adams, E. B. Carsten, and E. J. Lefkowitz (Elsevier, 2012), pp. 806–828.

[5] J. Cui, F. Li, and Z. L. Shi, "Origin and evolution of pathogenic coronaviruses," Nat. Rev. Microbiol. **17**, 181–192 (2019).

[6] G. Li and E. De Clercq, "Therapeutic options for the 2019 novel coronavirus (2019-nCoV)," Nat. Rev. Drug Discov. **19**, 149 (2020).

[7] L. Zhang and Y. Liu, "Potential interventions for novel coronavirus in China: A systematic review," J. Med. Virol. **92**, 479–490 (2020).

[8] H. Brüssow, "The novel coronavirus–A snapshot of current knowledge," Microb. Biotech. **13**, 607–612 (2020).

[9] B. Cao, Y. Wang, D. Wen, W. Liu, J. Wang, G. Fan, L. Ruan, B. Song, Y. Cai, M. Wei, and X. Li, "A trial of lopinavir–ritonavir in adults hospitalized with severe Covid-19," New Engl. J. Med. **382**, e68 (2020).

[10] M. Wang, R. Cao, L. Zhang, X. Yang, J. Liu, M. Xu, Z. Shi, Z. Hu, W. Zhong, and G. Xiao, "Remdesivir and chloroquine effectively inhibit the recently emerged novel coronavirus (2019-nCoV) in vitro," Cell Res. **30**, 269–271 (2020).

[11] J. Liu, R. Cao, M. Xu, X. Wang, H. Zhang, H. Hu, Y. Li, Z. Hu, W. Zhong, and M. Wang, "Hydroxychloroquine, a less toxic derivative of chloroquine, is effective in inhibiting SARS-CoV-2 infection in vitro," Cell Discov. **6**, 1–4 (2020).

[12] K. Anand, J. Ziebuhr, P. Wadhwani, J. R. Mesters, and R. Hilgenfeld, "Coronavirus main proteinase (3CLpro) structure: Basis for design of anti-SARS drugs," Science **300**, 1763–1767 (2003).

[13] L. Zhang, D. Lin, X. Sun, U. Curth, C. Drosten, L. Sauerhering, S. Becker, K. Rox, and R. Hilgenfeld, "Crystal structure of SARS-CoV-2 main protease provides a basis for design of improved α-ketoamide inhibitors," Science **368**, 409–412 (2020).

[14] B. Zhang, Y. Zhao, Z. Jin, X. Liu, H. Yang, and Z. Rao, "The crystal structure of COVID-19 main protease in apo form" (published online, 2020).

[15] H. X. Su, S. Yao, W. F. Zhao, M. J. Li, L. K. Zhang, Y. Ye, H. L. Jiang, and Y. C. Xu, "Identification of a novel inhibitor of SARS-CoV-2 3CLpro" (published online, 2020).

[16] Z. Jin, X. Du, M. Liu, Y. Zhao, B. Zhang, X. Li, L. Zhang, C. Peng, and Y. Duan, "Structure of Mpro from COVID-19 virus and discovery of its inhibitors," Nature (published online, 2020).

[17] W. Dai, B. Zhang, H. Su, J. Li, Y. Zhao, X. Xie, Z. Jin, F. Liu, C. Li, Y. Li, and F. Bai, "Structure-based design of antiviral drug candidates targeting the SARS-CoV-2 main protease," Science (published online, 2020).

[18] G. Amitai, A. Shemesh, E. Sitbon, M. Shklar, D. Netanely, I. Venger, and S. Pietrokovski, "Network analysis of protein structures identifies functional residues," J. Mol. Biol. **344**, 1135–1146 (2004).

[19] E. Estrada, "Universality in protein residue networks," Biophys. J. **98**, 890–900 (2010).

[20] W. I. Karain and N. I. Qaraeen, "The adaptive nature of protein residue networks," Proteins: Struct. Funct. Bioinf. **85**, 917–923 (2017).

[21] U. Doshi, M. J. Holliday, E. Z. Eisenmesser, and D. Hamelberg, "Dynamical network of residue–residue contacts reveals coupled allosteric effects in recognition, catalysis, and mutation," Proc. Natl. Acad. Sci. U.S.A. **113**, 4735–4740 (2016).

[22] C. F. Negre, U. N. Morzan, H. P. Hendrickson, R. Pal, G. P. Lisi, J. P. Loria, I. Rivalta, J. Ho, and V. S. Batista, "Eigenvector centrality for characterization of protein allosteric pathways," Proc. Natl. Acad. Sci. U.S.A. **115**, E12201–E12208 (2018).

[23] E. Estrada, *The Structure of Complex Networks: Theory and Applications* (Oxford University Press, 2012).

[24] V. Latora, V. Nicosia, and G. Russo, *Complex Networks: Principles, Methods and Applications* (Cambridge University Press, 2017).

[25] D. Helbing, D. Brockmann, T. Chadefaux, K. Donnay, U. Blanke, O. Woolley-Meza, M. Moussaid, A. Johansson, J. Krause, S. Schutte, and M. Perc, "Saving human lives: What complexity science and information systems can contribute," J. Stat. Phys. **158**, 735–781 (2015).

[26] K. Prem, Y. Liu, T. W. Russell, A. J. Kucharski, R. M. Eggo, N. Davies, S. Flasche, S. Clifford, C. A. Pearson, J. D. Munday, and S. Abbott, "The effect of control strategies to reduce social mixing on outcomes of the COVID-19 epidemic in Wuhan, China: A modelling study," Lancet Public Health **5**, E261–E270 (2020).

[27] G. Giordano, F. Blanchini, R. Bruno, P. Colaneri, A. Di Filippo, A. Di Matteo, and M. Colaneri, "Modelling the COVID-19 epidemic and implementation of population-wide interventions in Italy," Nat. Med. (published online, 2020).

[28] A. Arenas, W. Cota, J. Gómez-Gardenes, S. Gómez, C. Granell, J. T. Matamalas, D. Soriano-Panos, and B. Steinegger, "A mathematical model for the spatiotemporal epidemic spreading of COVID19," medRxiv 2020.03.21.20040022 (2020).

[29] M. Perc, N. Gorišek Miksić, M. Slavinec, and A. Stožer, "Forecasting Covid-19," Front. Phys. **8**, 127 (2020).

[30] A. Aleta, D. Martın-Corral, A. P. y. Piontti, M. Ajelli, M. Litvinova, M. Chinazzi, N. E. Dean, M. E. Halloran, I. M. Longini, Jr., S. Merler, A. Pentland, A. Vespignani, E. Moro, and Y. Moreno, "Modeling the impact of social distancing, testing, contact tracing and household quarantine on second-wave scenarios of the COVID-19 epidemic," medRxiv 2020.05.06.20092841 (2020).

[31] Protein Data Bank, The single global archive for 3D macromolecular structure data," Nucleic Acids Res. **47**, D520–D528 (2019).

[32] X. Xue, H. Yang, W. Shen, Q. Zhao, J. Li, K. Yang, C. Chen, Y. Jin, M. Bartlam, and Z. Rao, "Production of authentic SARS-CoV Mpro with enhanced activity: Application as a novel tag-cleavage endopeptidase for protein overproduction," J. Mol. Biol. **366**, 965–975 (2007).

[33] T. Muramatsu, C. Takemoto, Y. T. Kim, H. Wang, W. Nishii, T. Terada, M. Shirouzu, and S. Yokoyama, "SARS-CoV 3CL protease cleaves its C-terminal autoprocessing site by novel subsite cooperativity," Proc. Natl. Acad. Sci. U.S.A. **113**, 12997–13002 (2016).

[34] H. Yang, M. Yang, Y. Ding, Y. Liu, Z. Lou, Z. Zhou, L. Sun, L. Mo, S. Ye, H. Pang, and G. F. Gao, "The crystal structures of severe acute respiratory syndrome virus main protease and its complex with an inhibitor," Proc. Natl. Acad. Sci. U.S.A. **100**, 13190–5 (2003).

[35] J. Tan, K. H. Verschueren, K. Anand, J. Shen, M. Yang, Y. Xu, Z. Rao, J. Bigalke, B. Heisen, J. R. Mesters, and K. Chen, "pH-dependent conformational flexibility of the SARS-CoV main proteinase (Mpro) dimer: Molecular dynamics simulations and multiple X-ray structure analyses," J. Mol. Biol. **354**, 25–40 (2005).

[36] E. Estrada, "Quantifying network heterogeneity," Phys. Rev. E **82**, 066102 (2010).

[37] E. Estrada, "Degree heterogeneity of graphs and networks. I. Interpretation and the "heterogeneity paradox"," J. Interdisc. Math. **22**, 503–529 (2019).

[38]D. J. Watts and S. H. Strogatz, "Collective dynamics of 'small-world' networks," Nature **393**, 440–442 (1998).
[39]M. E. J. Newman and M. Girvan, "Finding and evaluating community structure in networks," Phys. Rev. E **69**, 026113 (2004).
[40]M. E. Newman, "Finding community structure in networks using the eigenvectors of matrices," Phys. Rev. E **74**, 036104 (2006).
[41]M. E. Newman, "Assortative mixing in networks," Phys. Rev. Lett. **89**, 208701 (2002).
[42]L. C. Freeman, "Centrality in social networks: Conceptual clarification," Soc. Netw. **1**, 215–239 (1979).
[43]P. Bonacich, "Power and centrality: A family of measures," Am. J. Soc. **92**, 1170–1182 (1987).
[44]E. Estrada and J. A. Rodriguez-Velazquez, "Subgraph centrality in complex networks," Phys. Rev. E **71**, 056103 (2005).
[45]E. Estrada and N. Hatano, "Communicability in complex networks," Phys. Rev. E **77**, 036111 (2008).
[46]E. Estrada and N. Hatano, "Communicability angle and the spatial efficiency of networks," SIAM Rev. **58**, 692–715 (2016).
[47]E. Estrada and G. Silver, "Accounting for the role of long walks on networks via a new matrix function," J. Math. Anal. Appl. **449**, 1581–1600 (2017).
[48]H. B. Mann and D. R. Whitney, "On a test of whether one of two random variables is stochastically larger than the other," Ann. Math. Stat. **18**, 50–60 (1947).
[49]Z. Wang and J. Zhang, "In search of the biological significance of modular structures in protein networks," PLoS Comput. Biol. **3**, e107 (2007).
[50]H. Yu, X. Zhu, D. Greenbaum, J. Karro, and M. Gerstein, "TopNet: A tool for comparing biological sub-networks, correlating protein properties with topological statistics," Nucleic Acids Res. **32**, 328–337 (2004).